

## Comparative Analysis of Porous Titanium Spinal Cage with Conventional Spinal Cages: A Finite Element Study

Prashant Kumar, Rahul Bhardwaj, Amrit Lal Matharu & Vijay Kumar Meena\*  
Manufacturing Science and Instrumentation, CSIR-CSIO, Sector 30C, Chandigarh 160 030, India

*Received 13 January 2023; revised 11 September 2023; accepted 19 September 2023*

The objective of this study is to compare the stress shielding effect of various conventional as well as modified additive manufactured porous materials used for spinal cages. A finite element study was performed by changing the design (fully porous and hybrid) and the materials (PEEK, CFR-PEEK, Titanium) of spinal cages. All the models were simulated under uniaxial compression, to study the stress shielding effect. The Finite Element Analysis results showed that the hybrid spinal cage transfers more stress to its adjacent vertebrae than the other design configurations under uniaxial compression. The hybrid titanium cage was most effective in reducing the stress shielding effect. The hybrid cage is stronger than PEEK & CFR-PEEK cages, however, due to the porous structure reduced stress shielding was observed.

**Keywords:** Additive manufacturing, CFR-PEEK, PEEK, PLIF, Ti6Al4V ELI

### Introduction

For many spinal disorders like degenerative disc disease, segmental instability, trauma, deformities of the spine, etc., interbody spine fusion surgery is the final treatment option. Degenerative disc disease is the most common diagnosis in various spinal disorders.<sup>1</sup> According to one study; approximately 83% of the surgeries performed on patients with degenerative spondylolisthesis used an interbody cage.<sup>2</sup>

Spinal fusion devices can be classified by different methods such as the approach of insertion i.e., posterior, anterior, lateral, oblique, or axial; by type of material i.e., Titanium alloy, Polyetheretherketone (PEEK), hybrid, etc. The lumbar interbody fusion techniques allow spinal surgeons to correct the coronal imbalance and other complications. The Posterior Lumbar Interbody Fusion (PLIF) procedure was introduced by Milligan and Briggs in 1944.<sup>(3)</sup> PLIF with cage insertion is a treatment method to achieve proper fusion and correct alignment in the coronal and sagittal plane, with the advantage of indirect foraminal decompression by raising disk height in lumbar degenerative diseases.<sup>4</sup> The fusion cages implanted in posterior surgical approaches are of smaller size than those used in oblique, anterior, and lateral surgical techniques. These cages typically rest on the lumbar endplate's central portion.<sup>5</sup>

Bagby proposed cage technology for spinal fusion in 1988.<sup>(6)</sup> Traditional solid cages of different materials such as titanium, PEEK, tantalum, etc. are frequently used in lumbar interbody fusion surgery. After the study of Stadelmann *et al.*<sup>7</sup>; which discovered the osseointegration linked with Titanium (Ti) implants, applications of solid Ti implants in the biomedical field, like dental and surgical fields, began. Ti implants are widely used in the spine because of their biocompatibility, formation of TiO<sub>2</sub> which promotes corrosion resistivity, and low density of approx. 4700 kg/m<sup>3</sup>.<sup>(8)</sup> While Ti had an advantage in terms of fusion rates; settling into host vertebral bodies due to differences in elastic modulus was a major disadvantage.<sup>9</sup> The elastic modulus of bone ranges from 1 to 20 GPa, whereas that of titanium is 110 GPa. The loading stresses are not passed through the implant to surrounding bone tissue as a result of this significant mismatch in elastic modulus, leading to stress shielding. This causes a reduction in mechanical stiffness of the bone and adaptive resorption of bone tissue as per Wolff's law.<sup>10,11</sup> The use of PEEK spinal cages in the biomedical implant market has grown as an alternative to a solid Ti cage since the Food and Drug Administration (FDA) approved it in 2001. PEEK is a hydrophobic polymer that has the same biomechanical properties as cancellous bone. On the other hand, it is chemically inert and performs poorly in protein absorption and cell adhesion. Wear along with fracture are major

\*Author for Correspondence  
E-mail: vijaykumar@csio.res.in

issues with PEEK implants, as they are with any load-bearing implant. Carbon Fiber-Reinforced PEEK (CFR-PEEK) with 30% CFR is used to increase wear resistance.<sup>12</sup> Some properties of titanium and PEEK cages are listed in Table 1.

Nemoto *et al.*<sup>14</sup> showed the fusion rate comparison of solid Ti cage and PEEK cage with the help of computed tomography and found that the Titanium group showed fusion in 96% of cases and the PEEK group showed it in 64% of cases at 12 months. The Titanium group's fusion rate after 24 months had increased to 100%, whereas only a 76% fusion rate was observed in the PEEK group. However, due to their high elastic modulus, solid titanium cages have a significant impact on the load transfer characteristics of the human spine. Many studies have studied and recommended porous additive manufactured cages for their structural stiffness close to that of bone and it helped in reducing stress shielding.<sup>15,16</sup>

The formation of a porous structure with high interconnectivity has the potential to improve its osseointegrative potential and bioactivity.<sup>17</sup> The osteoconductive porous titanium surface provides adequate friction for short-term stability whereas long-term stability is achieved by increased cell adhesion, which leads to bone ingrowth.<sup>18</sup> Taniguchi *et al.* studied bone growth in the porous structure of 300, 600, and 900 microns and recommended the pore size of 600  $\mu\text{m}$  for best bone in growth.<sup>19</sup> Cells on titanium proliferate more widely on titanium than on PEEK.<sup>20</sup> However, there are issues with subsidence difference and metal radiopacity, as well as Magnetic Resonance Imaging (MRI) artefacts.<sup>21</sup>

The load-sharing behavior of the spine in compression or in osteoporotic compression, and the stabilizing capacity of the various spinal implants can be effectively predicted by the Finite Element (FE) analysis.<sup>22</sup> Another study showed that graft material experienced significantly higher stresses with the PEEK spacer than with the solid Titanium spacer. The

titanium spacer produced higher endplate stress than the PEEK spacer.<sup>23</sup> Zhang *et al.*<sup>24</sup> used Finite Element Analysis (FEA) to compare solid and porous Ti cages with PEEK cages by mechanically calculating Young's modulus of the porous structure and assigning the calculated Young's modulus to the solid region. The study found that using a solid cage with a porous structure property improved cage stress and endplate stress. The porous spinal cage has biomechanical advantages over the PEEK cage, having a better fusion rate in clinical practice.<sup>20</sup>

However, very few studies have been done on a detailed biomechanical load comparison among the materials used for spinal cages like solid titanium, PEEK, CFR-PEEK, and porous Ti structures. In this study, the effects of conventional materials with additive manufactured Ti porous structures on stress concentration on the cage and load transfer on subsequent bone have been focused on and studied with the help of FEA.

**Materials and Methods**

FEA was used to evaluate the stress distribution and displacement in the cage models and constructed lumbar vertebrae. To create a CAD model of the lumbar spine, a sample patient dataset provided by the Simpleware Scan IP software was utilized, as shown in Fig. 1(a). Within the same software, the model of the L4-L5 vertebrae was isolated from the surrounding spine. Subsequently, additional smoothing and wrapping procedures were performed on the segmented model using the 3-Matic module

Table 1 — Comparison of Titanium and PEEK cages (Adapted from<sup>13</sup>)

| Property                      | Titanium    | Polyetheretherketone (PEEK) |
|-------------------------------|-------------|-----------------------------|
| Modulus                       | 100–110 GPa | 3.5 GPa                     |
| Radiodensity                  | Radiopaque  | Radiolucent                 |
| Subsidence rates              | Higher      | Lower                       |
| Promotion of osseointegration | Higher      | Lower                       |
| Metal allergy risk            | Yes         | No                          |

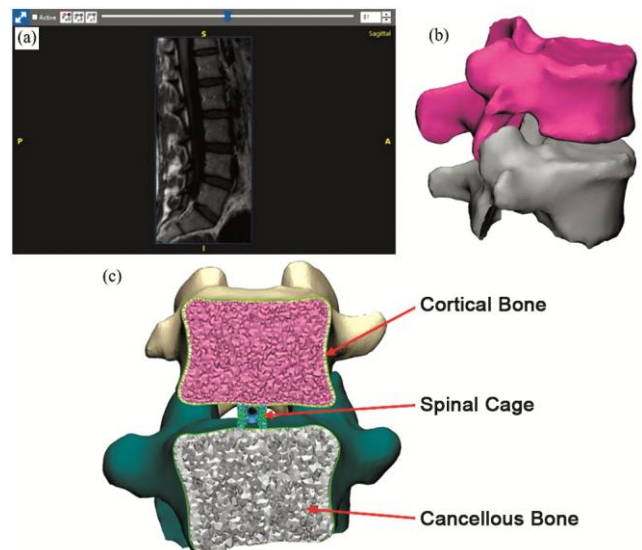


Fig. 1 — (a) Demo data of lumbar spine; (b) L4-L5 vertebra model; and (c) Section view of the assembly

within the Mimics Innovation Suite software. The resulting CAD representation of the L4-L5 vertebrae employed in this study is presented in Fig. 1(b). Each vertebra was split into two sections: cortical bone and cancellous bone. The cortical bone is the outer shell with a thickness of 1.0 mm<sup>25</sup> and the rest of the inner area was considered cancellous bone. A sectional cut of the assembly model is illustrated in Fig. 1(c), which includes L4-L5 vertebrae and the spinal cage.

The design of a commercially available PLIF spinal cage was taken as a reference to perform the study. The same design was used for PEEK, CFR-PEEK, and solid Ti spinal cages, however, were modified for hybrid and fully porous design. The hybrid cage consists of both porous and solid regions (Fig. 2(c)). The unit cell used in the porous part of both these designs (hybrid and fully porous) was a diamond unit cell with a pore size of 600 μm as shown in Fig. 2.<sup>(19)</sup>

A convergence analysis study was carried out prior to the meshing of the actual assembly model. The assembly model for convergence analysis with a solid spinal implant placed between two flat plates is modeled in 3-Matic software and mimics the actual assembly model. It is then meshed with 3D tetrahedra elements in Simpleware software (Fig. 3). Using a grading range from -50 to +50, Simpleware software determined the mesh's fineness and coarseness. The mesh got finer as the scale shifted from left to right i.e. from -50 to +50. Convergence analysis was conducted using four different meshing refinement levels: -20, -15, -10, and -5. Subsequently, all resulting meshes were imported into the Abaqus CAE software for finite element analysis (FEA). In each model, a uniaxial compression load of 400 N was

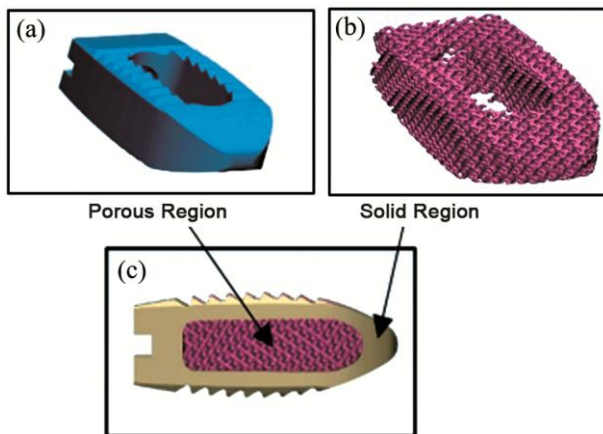


Fig. 2 — CAD model of: (a) Solid Cage, (b) Fully porous cage, and (c) Hybrid cage

uniformly applied to the upper plate's top surface, while the lower plate was fully constrained at its bottom. Both the plates and the solid implant have Ti6AL4V ELI material properties. The elements, nodes, and maximum stress values of the assembly model with corresponding grade value is listed in Table 2.

In Fig. 4, the grade value for meshing is plotted against the von-Mises stress value, and as observed from the graph, the stress values are convergent for grades -10 and -5. Therefore, a grade value of -10 is utilized to mesh the actual model because a grade value of -5 would require a longer simulation period.

The meshing of assembly models of L4-L5 vertebrae and the spinal cage was performed in Simpleware Scan IP 19.09 software. The 3D

Table 2 — Elements, nodes and maximum stress values of assembly model with corresponding grade value for meshing for the study of convergence analysis

| Grade value | Number of nodes | Number of elements | Maximum von-Mises stress (MPa) |
|-------------|-----------------|--------------------|--------------------------------|
| -20         | 1615            | 5452               | 16.85                          |
| -15         | 2081            | 7140               | 29.50                          |
| -10         | 2981            | 10440              | 36.33                          |
| -5          | 6771            | 25745              | 37.51                          |

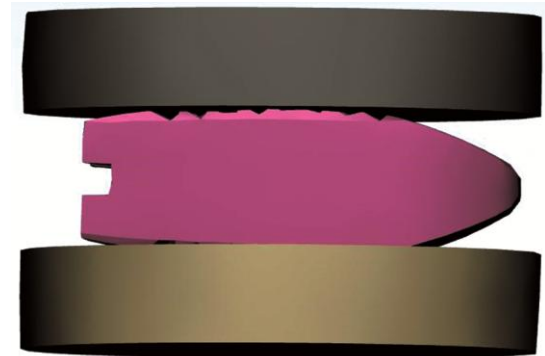


Fig. 3 — Assembly model for convergence analysis

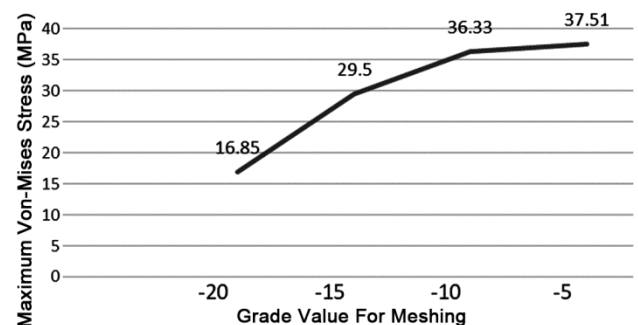


Fig. 4 — Convergence in von-Mises stress values with corresponding grade value for meshing

tetrahedral elements were used to mesh all the FE models. After meshing, the meshed models of the assembly were imported into Abaqus software for performing FEA. Mechanical properties were assigned to relevant bones and different material properties (PEEK, CFR-PEEK, titanium) were assigned to solid cages for the comparative study. All the studied design configurations are tabulated in Table 3.

The material properties of the porous titanium structure were assigned to the porous cage. The stiffness of a porous titanium structure is different from solid titanium. To determine Young’s modulus of the porous structure, a model of size 10 × 10 × 20 mm with a diamond unit cell having a pore size of 600 μm was designed in Simpleware software and additively manufactured in Ti6Al4V ELI metal powder with 30-micron layer height using an EOS M290 metal printer. The printer has a bed size of 250 × 250 × 325 mm and is equipped with 400 W Nd-YAG fiber laser. After the printing process, the printed models went under heat treatment at 800°C for 2 hours in argon atmosphere and then cut apart from

the base plate with the help of wire EDM. The porous samples were then tested using a Universal testing machine (UTM). Five samples were tested and the average Young’s modulus value was found to be 2423.43 MPa. The porous sample used for testing and the compression anvils is shown in Fig. 5. The material properties designated for the Finite Element Analysis (FEA) are presented in Table 4.

The loading and boundary conditions used for performing FEA are shown in Fig. 6. To check the stress transferred from one vertebra to another after spinal fusion surgery, a uniaxial compression load of 400 N<sup>31</sup> was applied on the upper surface of the L4 vertebra, and the lower surface of the L5 vertebra was given encastre boundary conditions (fully constrained). All of the assembly’s connections including the facet joints of vertebrae L4 and L5 were given tie constraints, to simulate the effect of the screw and rod.<sup>32</sup> Relative movements between the vertebrae are limited because of tie constraints between the facets, so the FE model was created without any ligaments.<sup>33,34</sup> These boundary conditions are consistent with data from the literature.<sup>32,35</sup>

Table 3 — Overview of design configurations for the comparative study

| Configurations | Design Variation/ Material  |
|----------------|---|
| M1             | PEEK  |
| M2             | CFR-PEEK  |
| M3             | Solid Titanium  |
| M4             | Solid Ti model with porous properties                                   |
| M5             | Fully Porous  |
| M6             | Hybrid (porous region having diamond unit cell and pore size of 600 μm) |

Table 4 — Material properties for FEA Study

| Components                       | Young’s Modulus (MPa) | Poisson Ratio |
|----------------------------------|-----------------------|---------------|
| Cortical Bone <sup>26,27</sup>   | 12000                 | 0.3           |
| Cancellous Bone <sup>26,27</sup> | 100                   | 0.2           |
| Titanium <sup>28,29</sup>        | 110000                | 0.3           |
| PEEK <sup>23,29</sup>            | 3500                  | 0.3           |
| CFR-PEEK <sup>30</sup>           | 18000                 | 0.3           |
| Porous Titanium (This study)     | 2423.43               | 0.3           |

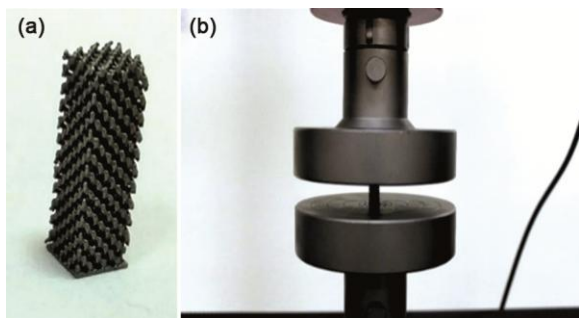


Fig. 5 — (a) Fabricated sample of porous titanium sample for Young’s modulus estimation; and (b) Tested sample between the compression anvils of UTM

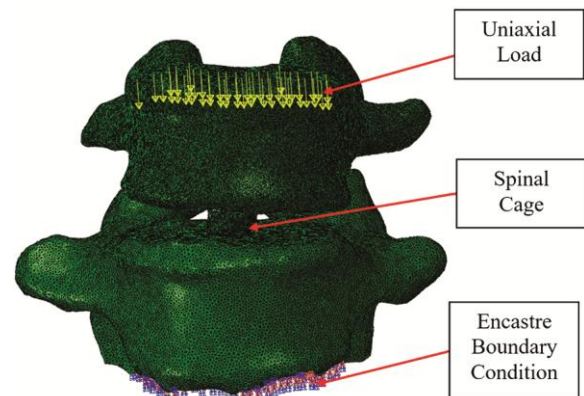


Fig. 6 — Loading and boundary conditions

Table 5 — Maximum von-Mises stress value and displacement value under uniaxial compression of 400N

| Configuration | Maximum von-Mises stress on the cage (MPa) | Maximum von-Mises Stress on L5 (MPa) | Maximum displacement of the cage (mm) | Maximum displacement of L5 (mm) |
|---------------|--|--------------------------------------|---------------------------------------|---------------------------------|
| M1            | 116.80                                     | 32.41                                | 0.0508                                | 0.00827                         |
| M2            | 136.30                                     | 30.00                                | 0.0196                                | 0.00682                         |
| M3            | 260.70                                     | 28.16                                | 0.0096                                | 0.00636                         |
| M4            | 130.80                                     | 31.87                                | 0.0509                                | 0.00848                         |
| M5            | 1753.00                                    | 124.20                               | 0.9304                                | 0.04030                         |
| M6            | 421.90                                     | 45.23                                | 0.0532                                | 0.00911                         |

## Results and Discussion

In this study, finite element methods are used to analyze the biomechanical properties of the cage fusion site and adjacent vertebrae when implanting spinal cages of various materials and designs. The images of stress distribution on the spinal cage and L5 vertebral bone were shown to depict the stress behavior and the stress transfer effect on the L5 vertebral bone. The maximum stress and displacement values observed on the spinal cage and L5 vertebra for various configurations are documented in Table 5. The von-Mises stress distribution and displacement distribution of different configurations under uniaxial compression loading are depicted in Table 6.

The values of maximum stress (von-Mises) on the spinal cage varied from 116.8 MPa to 1753 MPa for analyzed configurations. The highest value of von-Mises stress was found for a fully porous spinal cage (configuration M5) with a stress value of 1753 MPa which was more than the yield stress value of solid titanium and can result in mechanical failure. The high-stress values indicate the mechanical failure of configuration M5, so, the other results for this configuration are ignored for discussion and only the graphical representations are shown. The lowest value of von-Mises stress was found for the PEEK spinal cage (configuration M1) with a stress value of 116.8 MPa.

It is also evident from Table 5 that due to the addition of carbon fiber in PEEK, the load-bearing strength of CFR-PEEK is greater, however, this is achieved at the cost of increased stress shielding. The variation of stress values on the spinal cage for different configurations is shown in Fig. 7.

The values of maximum stress on the L5 vertebra varied from 28.16 MPa to 45.23 MPa for analyzed configurations. The highest value of stress was found for the hybrid spinal cage (configuration M6) which is 45.23 MPa and it can be deduced that the hybrid spinal cage has the best stress transfer characteristics to its adjacent vertebra. The lowest value of stress was

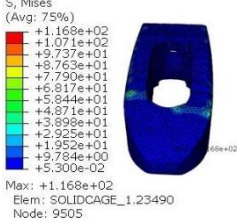
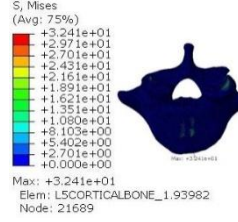
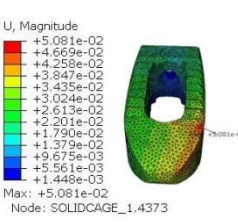
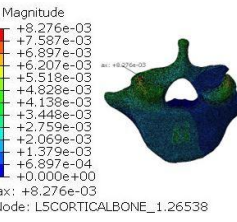
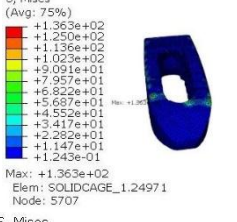

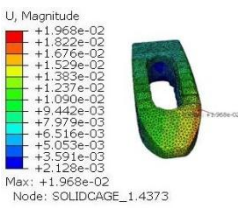
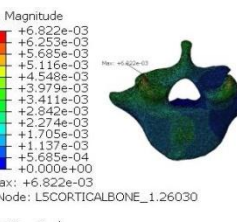
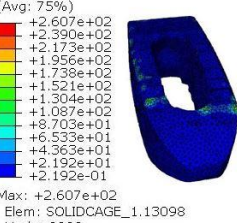
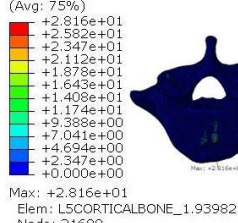
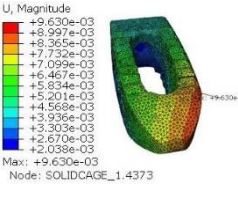
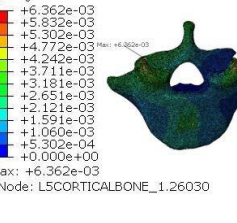
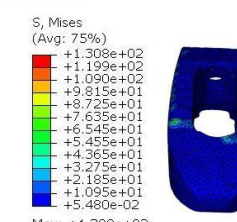
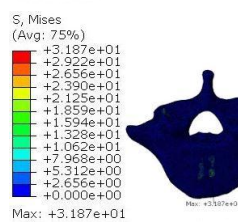
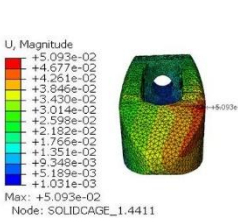
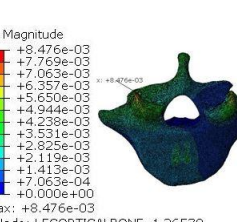
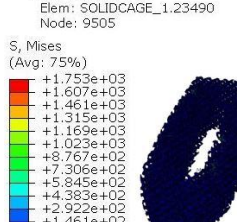
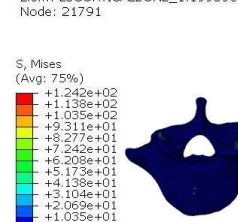
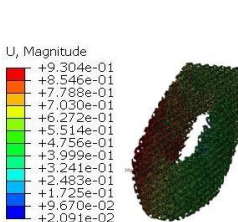
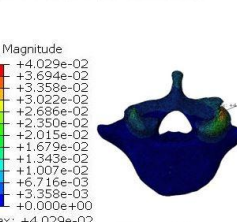

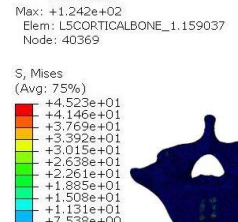
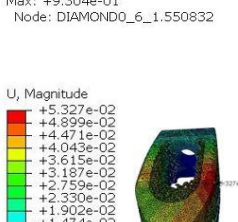

found for the solid Ti spinal cage (configuration M3) with a stress value of 28.16 MPa. The maximum stress values on the L5 vertebra for different configurations are shown in Fig. 8 in graphical form. The hybrid cage reduces stiffness through lattice structures and provides greater mechanical stimulation while maintaining stability. According to pertinent studies, the speed of bone regeneration can be greatly accelerated by mechanical stimulation, hence a hybrid titanium alloy cage fuses bones more quickly than a solid titanium alloy cage.

The values of maximum displacement of the spinal cage varied from 0.00963 mm to 0.0532 mm for analyzed configurations. The highest value of displacement was found for the hybrid cage (configuration M6) with a value of 0.0532 mm. The lowest value of displacement was found for the solid Ti spinal cage (configuration M3) with a maximum displacement value of 0.00963 mm. The graphical representation of the maximum displacement values of the spinal cage for different configurations is shown in Fig. 9.

According to Simon *et al.*, micro-movements greater than 0.150 mm weakened interface bonding strength, eventually leading to implant relaxation.<sup>36</sup> Because maximum cage displacement is regarded as a major factor for implant stability, the results show that all cage design configurations, with the exception of the fully porous one, can provide immediate stability.

The values of maximum displacement of the L5 vertebra varied from 0.00636 to 0.00911 mm for analyzed configurations. The highest value of displacement was found hybrid spinal cage (configuration M6) with a maximum displacement value of 0.00911 mm. The lowest value of displacement was found for the solid Ti spinal cage (configuration M3) with a maximum displacement value of 0.00636 mm. The graphical representation of the maximum values of displacement of the L5 vertebra for different configurations is shown in Fig. 10.

Table 6 — Von-Mises stress distribution and displacement distribution under uniaxial compression of 400 N

| Config-uration | Stress distribution in the cage   | Stress distribution on L5   | Displacement distribution of the cage   | Displacement distribution on L5  |
|----------------|---|---|---|--|
| M1             |  <p>S, Mises (Avg: 75%)<br/>                     Max: +1.168e+02<br/>                     Elem: SOLIDCAGE_1.23490<br/>                     Node: 9505</p>        |  <p>S, Mises (Avg: 75%)<br/>                     Max: +3.241e+01<br/>                     Elem: LSCORTICALBONE_1.93982<br/>                     Node: 21689</p>    |  <p>U, Magnitude<br/>                     Max: +5.081e-02<br/>                     Node: SOLIDCAGE_1.4373</p>       |  <p>U, Magnitude<br/>                     Max: +8.276e-03<br/>                     Node: LSCORTICALBONE_1.26538</p>   |
| M2             |  <p>S, Mises (Avg: 75%)<br/>                     Max: +1.363e+02<br/>                     Elem: SOLIDCAGE_1.24971<br/>                     Node: 5707</p>        |  <p>S, Mises (Avg: 75%)<br/>                     Max: +3.000e+01<br/>                     Elem: LSCORTICALBONE_1.54924<br/>                     Node: 21893</p>    |  <p>U, Magnitude<br/>                     Max: +1.969e-02<br/>                     Node: SOLIDCAGE_1.4373</p>       |  <p>U, Magnitude<br/>                     Max: +6.822e-03<br/>                     Node: LSCORTICALBONE_1.26030</p>   |
| M3             |  <p>S, Mises (Avg: 75%)<br/>                     Max: +2.607e+02<br/>                     Elem: SOLIDCAGE_1.13098<br/>                     Node: 9899</p>       |  <p>S, Mises (Avg: 75%)<br/>                     Max: +2.816e+01<br/>                     Elem: LSCORTICALBONE_1.93982<br/>                     Node: 21689</p>   |  <p>U, Magnitude<br/>                     Max: +9.630e-03<br/>                     Node: SOLIDCAGE_1.4373</p>      |  <p>U, Magnitude<br/>                     Max: +6.362e-03<br/>                     Node: LSCORTICALBONE_1.26030</p>  |
| M4             |  <p>S, Mises (Avg: 75%)<br/>                     Max: +1.308e+02<br/>                     Elem: SOLIDCAGE_1.23490<br/>                     Node: 9505</p>      |  <p>S, Mises (Avg: 75%)<br/>                     Max: +3.187e+01<br/>                     Elem: LSCORTICALBONE_1.199598<br/>                     Node: 21791</p> |  <p>U, Magnitude<br/>                     Max: +5.093e-02<br/>                     Node: SOLIDCAGE_1.4411</p>     |  <p>U, Magnitude<br/>                     Max: +8.476e-03<br/>                     Node: LSCORTICALBONE_1.26538</p> |
| M5             |  <p>S, Mises (Avg: 75%)<br/>                     Max: +1.753e+03<br/>                     Elem: DIAMONDDO_6_1.256992<br/>                     Node: 774028</p> |  <p>S, Mises (Avg: 75%)<br/>                     Max: +1.242e+02<br/>                     Elem: LSCORTICALBONE_1.159037<br/>                     Node: 40369</p> |  <p>U, Magnitude<br/>                     Max: +9.304e-01<br/>                     Node: DIAMONDDO_6_1.550832</p> |  <p>U, Magnitude<br/>                     Max: +4.029e-02<br/>                     Node: LSCORTICALBONE_1.27353</p> |
| M6             |  <p>S, Mises (Avg: 75%)<br/>                     Max: +4.219e+02<br/>                     Elem: SOLID_1.41978<br/>                     Node: 2327</p>          |  <p>S, Mises (Avg: 75%)<br/>                     Max: +4.523e+01<br/>                     Elem: LSCORTICALBONE_1.199598<br/>                     Node: 21791</p> |  <p>U, Magnitude<br/>                     Max: +5.327e-02<br/>                     Node: SOLID_1.6535</p>         |  <p>U, Magnitude<br/>                     Max: +9.115e-03<br/>                     Node: LSCORTICALBONE_1.27353</p> |

The superior material qualities of Ti6Al4V ELI were confirmed by the biomechanical comparison

results of the titanium alloy cages with other traditional cages. Although titanium cages effectively

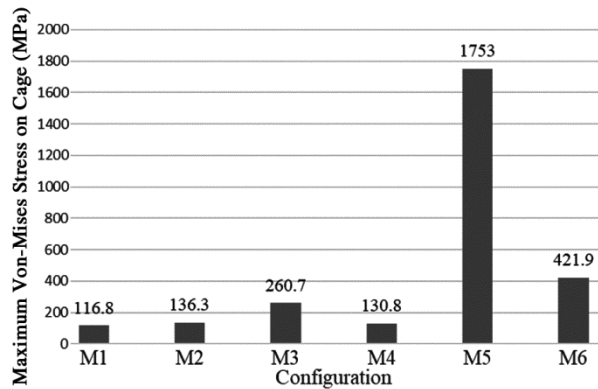


Fig. 7 — Maximum stress on cage for different configurations under uniaxial compression

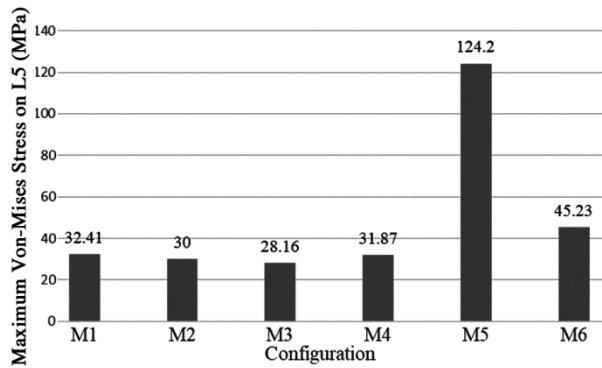


Fig. 8 — Maximum stress on L5 for different configurations under uniaxial compression

decrease the stress shielding effect, conventional solid cage stiffness remains higher than that of human bone. Structures with reduced stiffness should potentially lower the stress on adjacent intervertebral discs and facet joints.<sup>37,38</sup> The cage stiffness could be further reduced through structural design changes such as the introduction of porous lattice structures, bringing it even closer to the human bone. Simultaneously, the porous lattice structures can facilitate bone growth while accelerating the fusion of the spinal cage.

## Conclusions

In this work, a comparison of conventionally used materials in spinal cages i.e. titanium, PEEK, CFR-PEEK has been done with additive-manufactured porous and hybrid spinal cages. Young's modulus of the porous structure was mechanically tested and used for performing FEA analysis of porous and hybrid spinal implants. For conventional implant material values from the literature were taken. The following conclusions can be derived from this study:

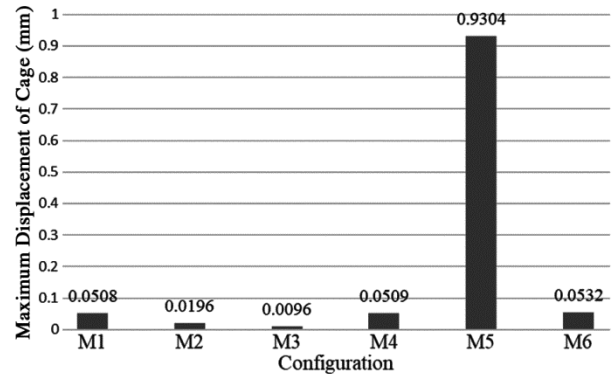


Fig. 9 — Maximum displacement of the cage for different configurations under uniaxial compression

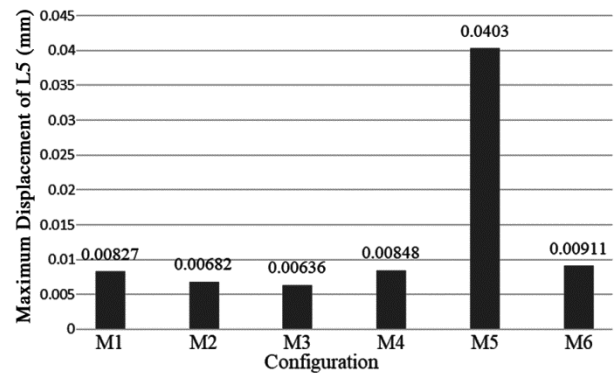


Fig. 10 — Maximum displacement of L5 for different configurations under uniaxial compression

(1) Young's modulus of diamond porous structure with 600  $\mu\text{m}$  pore size approximately matches Young's modulus of cancellous bone as well as that of PEEK.

(2) The fully porous spinal titanium cage design is not suitable for use due to low strength and failure when a 400 N load is applied.

(3) The hybrid titanium cage was most effective in reducing the stress shielding effect. While the hybrid cage exhibits greater strength compared to PEEK and CFR-PEEK cages, its porous structure leads to increased stress transfer to adjacent vertebrae, thereby diminishing the stress shielding effect typically associated with solid titanium.

Combining the advantages of cell adhesion, osteoconductive surface, bone growth, and improved stress shielding, the additive-manufactured hybrid porous-solid design is best suited for spinal fusion surgeries among the designs mentioned in this paper. This study can be beneficial for orthopaedic/neurological surgeons to choose the right material type of spinal cages.

The results of the FE study done in this work are limited by certain assumptions. To enhance

computational efficiency, the material properties of vertebrae were assumed to be linear elastic, even though these components are intrinsically nonlinear. In future study, *in vitro* mechanical static/dynamic testing can be performed on spinal cages.

### Conflict of Interest

There is no conflict of interest to declare.

### Acknowledgment

The financial support provided by ICMR, New Delhi, India under Grant no. 17x(3)/Adhoc/78/2022-ITR is acknowledged by the authors.

### References

- Pannell W C, Savin D D, Scott T P, Wang J C & Daubs M D, Trends in the surgical treatment of lumbar spine disease in the United States, *Spine J*, **15**(8) (2015) 1719–1727.
- Norton R P, Bianco K, Klifto C, Errico T J & Bendo J A, Degenerative spondylolisthesis: an analysis of the nationwide inpatient sample database, *Spine*, **40**(15) (2015) 1219–1227.
- Adams M A & Roughley P J, What is intervertebral disc degeneration, and what causes it?, *Spine*, **31**(18) (2006) 2151–2161.
- Park Y & Ha J W, Comparison of one-level posterior lumbar interbody fusion performed with a minimally invasive approach or a traditional open approach, *Spine*, **32**(5) (2007) 537–543.
- Gussous Y M, Jain N & Khan S N, Posterior based lumbar interbody fusion devices: Static and expandable technology, *Seminars in Spine Surgery:2018* (Elsevier), 2018, 203–206.
- Bagby & George W, Arthrodesis by the distraction-compression method using a stainless steel implant, *Orthopaedics*, **11**(6) (1988) 931–934.
- Stadelmann V A, Terrier A & Pioletti D P, Microstimulation at the bone-implant interface upregulates osteoclast activation pathways, *Bone*, **42**(2) (2008) 358–364.
- Ramakrishna S, Mayer J, Wintermantel E & Leong K W, Biomedical applications of polymer-composite materials: A review, *Compos Sci Technol*, **61**(9) (2001) 1189–1224.
- Karikari I O, Jain D, Owens T R, Gottfried O, Hodges T R, Nimjee S M & Bagley C A, Impact of subsidence on clinical outcomes and radiographic fusion rates in anterior cervical discectomy and fusion: A systematic review, *Clin. Spine Surg*, **27**(1) 2014 1–10.
- Chen J-H, Liu C, You L & Simmons C A, Boning up on Wolff's Law: Mechanical regulation of the cells that make and maintain bone, *J Biomech*, **43**(1) (2010) 108–118.
- Stock J T, Wolff's law (bone functional adaptation), *The International Encyclopedia of Biological Anthropology* (Wiley:Hoboken, NJ, USA) 2018, 1–2.
- Kurtz S M, Development and clinical performance of PEEK intervertebral cages, *PEEK Biomaterials Handbook* (Elsevier) 2019, 263–280.
- Seaman S, Kerezoudis P, Bydon M, Torner J C & Hitchon P W, Titanium vs. polyetheretherketone (PEEK) interbody fusion: meta-analysis and review of the literature, *J Clin Neurosci*, **44** (2017) 23–29.
- Nemoto O, Asazuma T, Yato Y, Imabayashi H, Yasuoka H & Fujikawa A, Comparison of fusion rates following transforaminal lumbar interbody fusion using polyetheretherketone cages or titanium cages with transpedicular instrumentation, *Eur Spine J*, **23**(10) (2014) 2150–2155.
- Kanayama M, Cunningham B W, Haggerty C J, Abumi K, Kaneda K & McAfee P C, *In vitro* biomechanical investigation of the stability and stress-shielding effect of lumbar interbody fusion devices, *J Neurosurg Spine*, **93**(2) (2000) 259–265.
- Herrera A, Yáñez A, Martel O, Afonso H & Monopoli D, Computational study and experimental validation of porous structures fabricated by electron beam melting: A challenge to avoid stress shielding, *Mater Sci Eng C*, **45** (2014) 89–93.
- Tsai P I, Hsu C C, Chen S Y, Wu T H & Huang C C, Biomechanical investigation into the structural design of porous additive manufactured cages using numerical and experimental approaches, *Comput Biol Med*, **76** (2016) 14–23.
- McGilvray K C, Easley J, Seim H B, Regan D, Berven S H, Hsu W K, Mroz T E & Puttlitz C M, Bony ingrowth potential of 3D-printed porous titanium alloy: A direct comparison of interbody cage materials in an *in vivo* ovine lumbar fusion model, *Spine J*, **18**(7) (2018) 1250–1260.
- Taniguchi N, Fujibayashi S, Takemoto M, Sasaki K, Otsuki B, Nakamura T, Matsushita T, Kokubo T & Matsuda S, Effect of pore size on bone ingrowth into porous titanium implants fabricated by additive manufacturing: An *in vivo* experiment, *Mater Sci Eng C*, **59** (2016) 690–701.
- Wu S H, Li Y, Zhang Y Q, Li X K, Yuan C F, Hao Y L, Zhang Z Y & Guo Z, Porous titanium-6 aluminum-4 vanadium cage has better osseointegration and less micromotion than a poly-ether-ether-ketone cage in sheep vertebral fusion, *Artif Organs*, **37**(12) (2013) E191–E201.
- Lim K M, Park T H, Lee S J & Park S J, Design and biomechanical verification of additive manufactured composite spinal cage composed of porous titanium cover and PEEK body, *Appl Sci*, **9**(20) (2019) 4258.
- Pitzen T, Geisler F, Matthis D, Müller-Storz H, Barbier D, Steudel W I & Feldges A, A finite element model for predicting the biomechanical behaviour of the human lumbar spine, *Control Eng Pract*, **10**(1) (2002) 83–90.
- Vadapalli S, Sairyo K, Goel V K, Robon M, Biyani A, Khandha A & Ebraheim N A, Biomechanical rationale for using polyetheretherketone (PEEK) spacers for lumbar interbody fusion—A finite element study, *Spine*, **31**(26) (2006) E992–E998.
- Zhang Z, Li H, Fogel G R, Liao Z, Li Y & Liu W, Biomechanical analysis of porous additive manufactured cages for lateral lumbar interbody fusion: A finite element analysis, *World Neurosurg*, **111** (2018) e581–e591.
- Ambati D V, Wright Jr E K, Lehman Jr R A, Kang D G, Wagner S C & Dmitriev A E, Bilateral pedicle screw fixation provides superior biomechanical stability in transforaminal lumbar interbody fusion: A finite element study, *Spine J*, **15**(8) (2015) 1812–1822.



- 26 Shirazi-Adl A, Ahmed A M & Shrivastava S C, Mechanical response of a lumbar motion segment in axial torque alone and combined with compression, *Spine*, **11(9)** (1986) 914–927.
- 27 Zhong Z C, Wei S H, Wang J P, Feng C K, Chen C S & Yu C H, Finite element analysis of the lumbar spine with a new cage using a topology optimization method, *Med Eng Phys*, **28(1)** (2006) 90–98.
- 28 Chosa E, Goto K, Totoribe K & Tajima N, Analysis of the effect of lumbar spine fusion on the superior adjacent intervertebral disk in the presence of disk degeneration, using the three-dimensional finite element method, *Clin Spine Surg*, **17(2)** (2004) 134–139.
- 29 Xiao Z, Wang L, Gong H & Zhu D, Biomechanical evaluation of three surgical scenarios of posterior lumbar interbody fusion by finite element analysis, *Biomed Eng Online*, **11(1)** (2012) 31.
- 30 Fan D Y, Li Y, Wang X, Zhu T J, Wang Q, Cai H, Li W S, Tian Y & Liu ZJ, Progressive 3D printing technology and its application in medical materials, *Front Pharmacol*, **11** (2020) 12.
- 31 Kurutz M, Finite element modelling of human lumbar spine, In: *Finite Element Analysis* (Editor: David Moratal) (IntechOpen, London) 2010, 209–236.
- 32 Epasto G, Distefano F, Mineo R & Guglielmino E, Subject-specific finite element analysis of a lumbar cage produced by electron beam melting, *Med Biol Eng Comput*, **57(12)** (2019) 2771–2781.
- 33 Choi K C, Ryu K S, Lee S H, Kim Y H, Lee S J & Park C K, Biomechanical comparison of anterior lumbar interbody fusion: stand-alone interbody cage versus interbody cage with pedicle screw fixation—a finite element analysis, *BMC Musculoskelet Disord*, **14(1)** (2013) 1–9.
- 34 Zhang Q H, Zhou Y L, Petit D & Teo E C, Evaluation of load transfer characteristics of a dynamic stabilization device on disc loading under compression, *Med Eng Phys*, **31(5)** (2009) 533–538.
- 35 Goel V, Monroe B, Gilbertson L & Brinckmann P, Interlaminar shear stresses and laminae separation in a disc: finite element analysis of the L3-L4 motion segment subjected to axial compressive loads, *Spine*, **20(6)** (1995) 689–698.
- 36 Simon U, Augat P, Ignatius A & Claes L, Influence of the stiffness of bone defect implants on the mechanical conditions at the interface — a finite element analysis with contact, *J Biomech*, **36(8)** (2003) 1079–1086.
- 37 Panjabi M M, Crisco J J, Vasavada A, Oda T, Cholewicki J, Nibu K & Shin E, Mechanical properties of the human cervical spine as shown by three-dimensional load – displacement curves, *Spine*, **26(24)** (2001) 2692–2700.
- 38 Lee J H, Park W M, Kim Y H & Jahng T A, A biomechanical analysis of an artificial disc with a shock-absorbing core property by using whole-cervical spine finite element analysis, *Spine*, **41(15)** (2016) E893–E901.